9

Advanced Robotic Radiative Process Control for Automotive Coatings

Fan Zeng and Beshah Ayalew
Clemson University - International Center for Automotive Research
United States of America

1. Introduction

In modern automotive manufacturing, coating, drying and curing processes provide essential protection for car bodies besides decorative functions. However, current coating and curing processes largely involve the use of convection bake-ovens and contribute immensely to the energy consumption and greenhouse gas emissions. For example, according to a recent study (Siewert, 2008), the total energy consumption per car manufactured averages about 3 MW-hr, of which 1.0-1.4 MW-hr (33-46%) happens in the painting/coating booth. Likewise, of the nearly 1.1 tons of CO_2 emissions per car manufactured, 0.4 tons (37%) of CO_2 emissions arise in the painting booths (Prendi et al., 2008). Assuming even the lowest industrial energy costs and considering the total annual global sales of nearly 70 million cars, estimated energy costs of painting booth operations alone run into trillions of dollars, not to mention the emission of tens of millions of tons of CO_2 into the atmosphere.

The energy and environmental issues involved in current automotive coating/paint curing processes may be alleviated by recent radiation-based methods which use either ultraviolet (UV) or infrared (IR) radiation to activate/initiate the curing or drying processes (Hagood et al., 2008) (Vgot, 2007). Compared to convection bake-ovens (Fig. 1a), these radiation-based methods use less energy, give improved productivity, and produce less air pollutions, such as CO_2, volatile organic compounds (VOCs), etc. As an example, a case study reported in (U.S. Department of Energy, 2003) showed that the replacement of the convection oven by a new IR oven allowed a metal finishing plant to increase its production by 50% and reduce natural gas consumption by 25% annually. Another study showed that the implementation

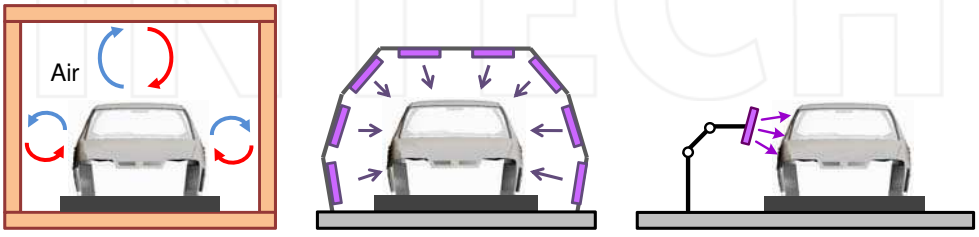

a. Convective Oven b. Fixed Radiant Array c. Robotic Radiant Array

Fig. 1. Alternative automotive paint curing processes

of UV-curable coatings for aluminum can production may save as much as 55% in capital and installation costs over thermal curing and reduce 47,000 tons / year of CO_2 emission if implemented industry-wide (U.S. Department of Energy, 1999).

Early applications of radiation-based methods (e.g. UV) in the automotive industry can be found in curing coated components, such as headlamp lenses, reflectors, instrument panels, and so on (Starzmann, 2001). The application of UV curing to whole car bodies (clearcoat) was reported in (Mills, 2001) and (Fey, 2003), in which the coated car bodies were enclosed and cured by a set of fixed UV lamps with predesigned positions and orientations (Fig. 1b). Industrial robotic manipulators have also been used in curing automotive parts and whole car bodies for further improvements in process quality and energy efficiency (Raith et al., 2001) (Mills, 2005). In these applications, the robotic manipulator is used to move the UV radiative device (e.g. UV lamp or LED panel attached to the end effector of the robot) around the target object in a pre-designed path (Fig. 1c). To ensure the curing quality, both off-line simulations (for process analysis and path design) and online trial tests (for irradiance measurement and parameter tuning) should be done before the curing system is implemented in actual production lines (Raith et al., 2001) (Mills, 2005).

However, the open-loop control structure of current robotic UV curing applications, including the off-line simulations and online trail tests described above, has difficulties in maintaining the desired quality during actual processes due to the presence of various disturbances. These include unevenness in UV absorption, geometrical variations, changes in convective environment etc. In addition, for these open-loop methods, the change in product shapes and materials not only requires the redesign of the path of the robot manipulator, but it also causes the repetitive and time-consuming trail tests for calibrating the curing process.

Compared to typical trial-and-error methods (open-loop), closed-loop control of robotic actuated processes have been widely used in various industrial applications, such as welding (Hardt, 1993) (Huissoon et al., 1994) (Moore et al., 1997), painting (Seelinger et al., 1997) (Omar et al., 2006), spray forming (Jones et al., 2003), and so on. For the robotic UV curing of automotive coatings discussed in this chapter, the authors have developed some closed-loop methods, including 1) feedback control through thermal imaging (Zeng & Ayalew, 2009), 2) online process state and parameter estimation (Zeng & Ayalew, 2010-a), and 3) multi-variable coordination and optimization (Zeng & Ayalew, 2010-b), in order to improve the process quality and energy efficiency. These closed-loop control and estimation methods will be detailed in this chapter.

The rest of the chapter is organized as follows. The second section describes the fundamental modelling and feedback control design for the robotic UV curing process. The third section details the design of a state/parameter estimator for online monitoring of the curing process. This is followed by a section which discusses two fundamental approaches to achieve optimization of the curing process, and a section that describes a prototype robotic UV curing system developed for experimental implementation. Finally, the last section gives the summary and points out future research directions.

2. Process modelling and feedback control design

This section describes the modelling of the robotic UV paint curing process and the design of a set of closed-loop control strategies through cure-status feedback. Despite the complex geometries of automotive parts or whole car bodies, the UV lamp/LED moving with the

robotic end effector only illuminates a small region of the whole target at a certain time and the dominant radiation usually occurs in the normal direction of that region. Therefore, for the currently illuminated region, the 3D curing process can be reduced to a 2D problem as illustrated in Fig. 2. The following subsections detail the modelling of the curing process and the feedback control design based on this 2D description.

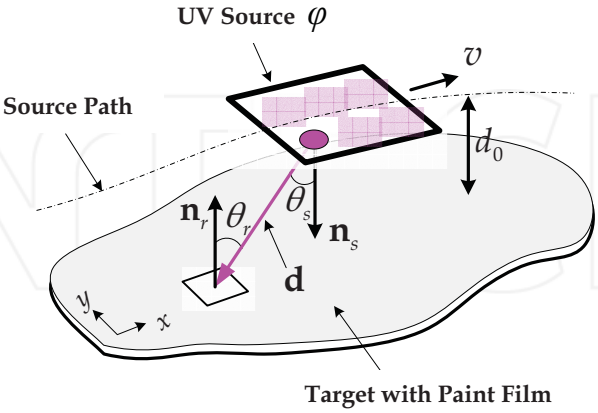

Fig. 2. The reduced schematic of a robotic UV curing process for a 2D target

2.1 Modeling the robotic UV curing process

In general, the UV curing mechanism can be broken into three coupled physical processes: irradiation, photo-initiated polymerization, and thermal evolution. Given the 2D schematic shown in Fig. 2, the mathematical description of the three fundamental processes is detailed as follows.

2.1.1 Irradiation

The major energy of the UV source is delivered to the target through radiation. The irradiance (power density) received by the target is strongly determined by the power level of the UV source and the relative distance and orientation between the source and the target. In this work, an LED type UV source is selected for its high efficiency and fast on-off response. As shown in Fig. 2, the LED UV source is composed of a set of small units and each unit can be modeled as a monochromatic Lambertian point source (Ashdown, 1994). Since the LED is an incoherent light source, the total irradiance arriving at the target surface can be obtained by superposition. Given the notations used in Fig. 2, the irradiance distribution on the target surface is represented by (Modest, 1993):

$$I(x,y,t)=\sum_{i=1}^{N} k(x,y)\frac{\varphi(t)\cos\theta_s^i(x,y,t)\cos\theta_r^i(x,y,t)}{N\pi\left|\mathbf{d}_i(x,y,t)\right|^2} \tag{1}$$

where, the spatial coordinates for an arbitrary point on the target surface and the time are denoted by (x , y) and t , respectively. The irradiance distribution on the target surface is represented by $I(x,y,t)$. The number of the LED units and the index of each unit are denoted by N and i , respectively. The relative distance and orientation between each LED

unit and the target surface are characterized by d_i (position vector), θ_s^i (emission angle), and θ_r^i (incidence angle). The total power level of the UV LED is represented by the radiant flux $\varphi(t)$. The coefficient $k(x,y)$ is used to model the varying UV absorption throughout the target surface. It can be observed from equation (1) that the irradiance received by the target varies with both time and coordinate. This characteristic will also strongly influence the photo-initiated polymerization and thermal evolution processes to be described later.

2.1.2 Photo-initiated polymerization

Most curing processes involve the polymerization of various monomers. In the UV curing process, the polymerization is initiated by the UV radiation instead of high temperature. A typical photo-initiated polymerization is composed of three fundamental phases: initiation, propagation, and termination. In initiation, the photo-initiators (mixed with the paint) absorb the UV radiation and create free radicals which initiate the growth of polymer chain. Propagation follows cross-linking more polymer chains. Termination occurs when growing chains come together and react to form the dead polymer. Detailed description of the photo-initiated polymerization can be found in (Hong, 2004) (Goodner, 2002). A simplified kinetic model is used here to characterize the three fundamental phases of the photo-initiated polymerization (Hong, 2004).

$$\frac{d[PI](x,y,t)}{dt} = -\phi\varepsilon[PI](x,y,t)I(x,y,t) \tag{2}$$

$$\begin{aligned}&\frac{d[M](x,y,t)}{dt}\\ &= -\frac{k_p}{k_t^{0.5}}(\phi\varepsilon)^{0.5}[M](x,y,t)\{[PI](x,y,t)\}^{0.5}\{I(x,y,t)\}^{0.5}\end{aligned} \tag{3}$$

where, the concentrations of photo-initiator and monomer are denoted by $[PI]$ and $[M]$. ϕ and ε represent the quantum of yield for initiation and molar absorptivity, respectively. The propagation and termination rate constants are denoted by k_p and k_t. It can be seen from equations (2) and (3) that the spatial distributions of both the photo-initiator and monomer concentrations are highly influenced by the distribution the UV irradiance.

2.1.3 Thermal evolution

The thermal evolution in the curing process is characterized by the following energy balance equation:

$$\begin{aligned}&\rho c\frac{dT(x,y,t)}{dt}\\ &= \nabla\{\lambda\nabla T(x,y,t)\} - \Delta H\frac{d[M](x,y,t)}{dt} - h\{T(x,y,t) - T_\infty\}\end{aligned} \tag{4}$$

In equation (4), the internal energy accumulation (described by the intensity ρ, specific heat capacity c, and the change of temperature T) is determined by the heat conduction throughout the target (λ and ∇ denote the thermal conductivity and the gradient operator, respectively), the heat generation in the photo-initiated polymerization phase (ΔH is the

polymerization enthalpy), and heat convection between the target and the environment (h and T_∞ denote the convective heat transfer coefficient and the ambient temperature, respectively). All radiative heat transfer terms are ignored in this energy balance equation as they are assumed to be comparatively smaller than the retained terms.

2.2 Feedback control design

Given the system dynamics modeled in subsection 2.1, the objective of the feedback control design is to take some of those measurable process outputs as feedback and manipulate the radiant source (either in motion or power) so that the desired process quality set-point can be achieved. In the present case, since the cure-conversion level (normalized monomer concentration) is usually difficult to measure directly, the temperature, which is highly correlated to the cure-conversion, can be used to provide on-going curing status information for the controller. The temperature can be measured through one or more infrared (IR) cameras. The following paragraphs will detail the use of temperature feedback and the corresponding feedback control design.

2.2.1 Temperature feedback through infrared (IR) cameras

The principle of temperature measurement through IR cameras is a form of thermal imaging, in which the IR camera captures the images of the target in the infrared frequency domain and correlates them to the temperature distribution of the target based on fundamental radiative heat transfer theory. Three possible configurations (as shown in Fig.3) can be used to implement online temperature measurement through IR cameras for the purpose of robotic process control.

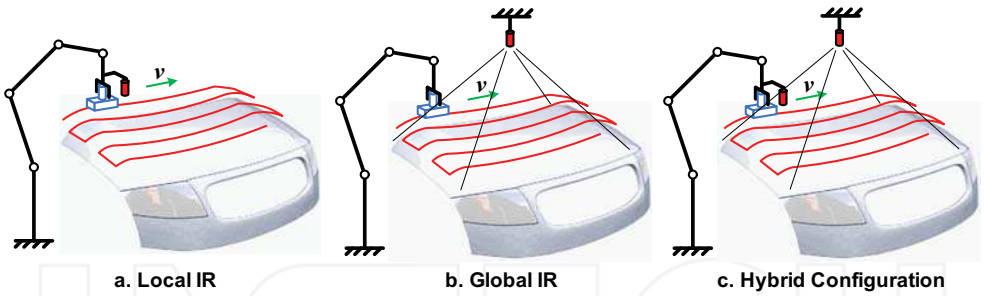

Fig. 3. Alternative temperature measurement configurations through IR cameras

In the local IR configuration (Fig. 3a), the IR camera is co-located with the moving radiant source, so it mainly focuses on the area which is currently being cured. This configuration is simple and effective for local temperature measurement. In the global IR configuration, the IR camera is fixed to the global coordinate system (e.g. test bench) so that it can have a full view of the target. With this configuration, the controller can receive more information from the IR camera (e.g. the complete temperature map of the target), but it also increases the image processing complexity. The hybrid configuration combines both the advantages of both the local and global ones, and it can help achieve better control performance with moderate cost compromise. The authors have developed different feedback control strategies for these alternative temperature measurement configurations, and the following subsection will give an overview of these strategies.

2.2.2 Control of the motion or power of the radiant source

With the temperature feedback obtained via the IR camera(s), some closed-loop control strategies are developed to improve the disturbance rejection capability of the system. In these closed-loop control strategies, only one of the two major manipulated variables (motion and power) of the radiant source is regulated online and the other is calibrated off-line or kept constant during the process. The general structure for these control strategies is illustrated in Fig. 4.

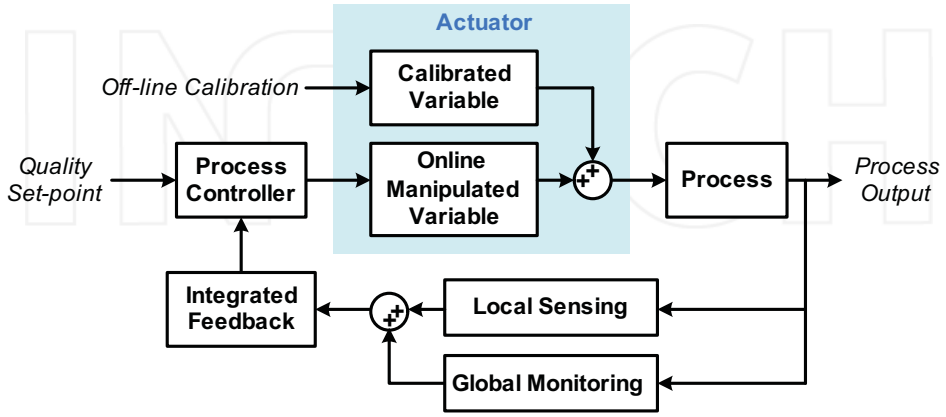

Fig. 4. The general output (temperature) feedback control structure

The control structure in Fig. 4 provides the framework for designing feedback control strategies based on different temperature measurement configurations depicted in Fig. 3. For the local IR configuration, a sequential curing style is selected, in which the radiant source stays at each segment of the target for a while and moves to the next one after the current segment has been cured. In this case, the power of the UV source is kept constant, while the motion of the robot is adjusted online (the controller determines the curing time for each segment based on the corresponding temperature level of the same segment, and commands the robot when it should move to the next one). For the global IR configuration, the radiant source is moved by the robot in a continuous manner, but the complete curing process is divided into several runs. The IR camera captures the temperature map of the target at the end of each run, and the controller decides if it is necessary to adjust the trajectory of the robot based on the global temperature feedback. The power of the UV source is still kept constant during the process for this configuration. For the hybrid configuration, the local and global temperature measurements are integrated into a real-time control structure, in which either the motion or the power of the radiant source can be adjusted continuously at any time of the process based on the integrated temperature feedback.

In these strategies above, the controller uses online temperature measurements directly to determine the appropriate motion or power applied to the radiant source. This can improve the process quality to some extent. However, the correlation between the temperature (process output, measured by IR cameras) and the cure-conversion level (controlled variable, difficult to be measured online) still needs to be calibrated through experiments. In the next section, an online estimator is developed to obtain such information by using a process model and the Kalman filtering method.

3. Online process state/parameter estimation

State/parameter estimation has been widely used for various industrial process control applications. For the automotive robotic UV curing, the development of a process estimator faces two major challenges. First, the target state (cure-conversion level) of the process is a spatially distributed variable and requires a large dimensional estimator. This may increase the computational cost. Second, the spatial movement of the radiant source can change the observability of the system. This has a signifciant influence on the estimation performance and it has to be carefully considered when designing the process estimator. This section details the development of a process state/parameter estimation scheme and discusses proposed solutions to the two major issues (large dimension and changing observability) described above.

3.1 Model reduction and simplification

To illustrate the development of the process estimator, the authors consider using a one-dimensional (1D) description (as shown in Fig. 5) to further simplify the robotic UV paint curing process depicted in Fig. 2.

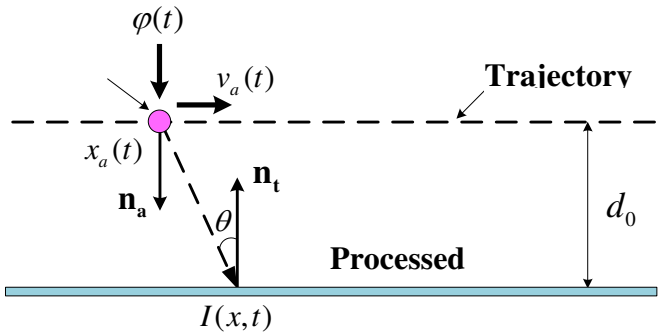

Fig. 5. The 1D description of the robotic UV paint curing process

In this 1D description, the actual UV radiant device is simplified as a point source. The variation along the cross-section direction is also ignored at this time. In addition, only a small segment of the processed target is considered here, so the 2D processed target has been reduced to a 1D strip. Then the corresponding process model can be reduced and simplified. For example, the simplified irradiation phase can be written as follows:

$$I(x,t) = k(x)\frac{\varphi(t)d_0^2}{\pi\left\{\left[x_a(t)-x\right]^2 + d_0^2\right\}^2} \tag{5}$$

Similar reduction and simplification can be applied to the photo-initiated polymerization and the thermal evolution phases. The detailed equations can be found in (Zeng & Ayalew, 2010-a).

3.2 Development of the state/parameter estimation scheme

This subsection describes the development of the state/parameter estimation scheme by using the dual extended Kalman filtering (DEKF) method. The main advantage of this method is that

it can help improve estimation accuracy by estimating some unknown process parameters, and subsequently correcting the process model that is used for estimation. Considering the two issues (large dimension and changing observability) mentioned at the beginning of this section, the authors develop the state/parameter estimation scheme keeping in mind the spatially distributed nature of the robotic radiative curing process.

3.2.1 Design of the dual extended Kalman filter (DEKF)

The dual extended Kalman filter (Wan and Nelson, 1997) is one of several variants of the original Kalman filter (Kalman, 1960), which provides combined state and parameter estimation through the use of two extended Kalman filters (EKFs) in parallel. Both EKFs follow the standard two-step (prediction and correction) estimation procedure. For the robotic UV curing process, the target state to be estimated is the monomer concentration, and the unknown process parameters considered here include the UV absorption coefficient and the convective heat transfer coefficient of the target. The basic structure of the DEKF adopted for this work is illustrated in Fig. 6.

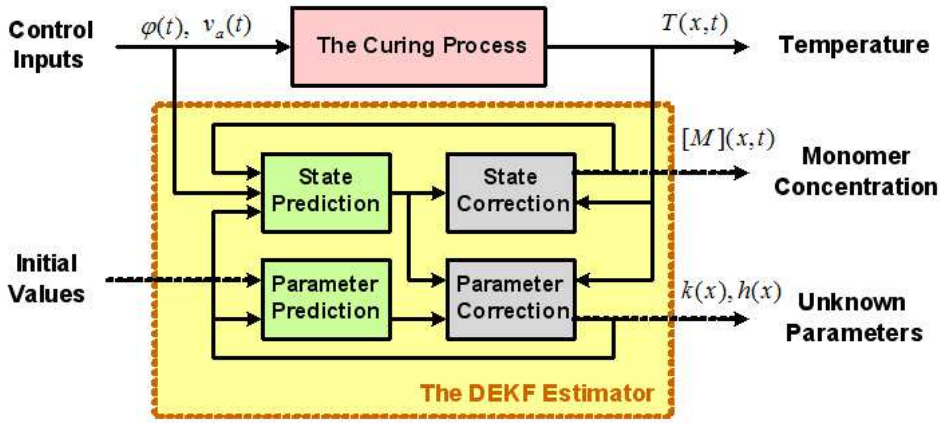

Fig. 6. The structure of the DEKF estimator

In Fig. 6, the two major inputs (power and motion) of the system are denoted by $\varphi(t)$ and $v_a(t)$. The output of the system is the temperature ($T(x,t)$), which can be measured online through IR cameras. The objective is to estimate the target state $[M](x,t)$ from the known inputs and the measured output. Parameter estimation is also applied to unknown process parameters ($k(x)$, $h(x)$) to improve the accuracy of the process model and further improve the state estimation performance.

The following formulation outlines the two-step (prediction and correction) estimation procedure adopted for this application. More details about the standard procedure for Kalman filter can be found in (Kalman, 1960) (Haykin, 2001).

Parameter Prediction:
$$\hat{\mathrm{p}}^{-}(j) = \hat{\mathrm{p}}(j-1) \tag{6}$$

State Prediction:
$$\hat{\mathrm{x}}^{-}(j) = F\left[\hat{\mathrm{x}}(j-1), \mathrm{u}(j-1), \hat{\mathrm{p}}(j-1)\right] \tag{7}$$

State Correction: $$\hat{x}(j) = \hat{x}^{-}(j) + K_s\left[y(j) - C\hat{x}^{-}(j)\right] \quad (8)$$

Parameter Correction: $$\hat{p}(j) = \hat{p}^{-}(j) + K_p\left[y(j) - C\hat{x}^{-}(j)\right] \quad (9)$$

where, the discrete time index is denoted by j. The state and parameter vectors to be estimated are represented by x and p, respectively. The input vector is denoted by u, and the measured output is represented by **y**. At the first step, only the state vector is updated by using the process model, which is described by a nonlinear function ($F(\cdot)$) of the state, input, and parameter vectors at the previous time $j-1$. At the second step, the state and parameter vectors obtained at the prediction step will be further corrected based on current process output measurements. Two Kalman gain matrices (K_s and K_p, corresponding to state and parameter, respectively) are used here to weigh the prediction and correction parts, and give the final estimates at time j. The two gain matrices are also updated with time by following the standard procedure.

3.2.2 Implementation of the DEKF estimation scheme

Two major issues should be considered when implementing the DEKF estimation scheme to the robotic UV curing process: the large dimension of the estimator and the changing observability of the system caused by the moving radiant source. The detailed derivation and discussion on the changing observability can be found in the authors' previous work in (Zeng and Ayalew, 2010-a). To resolve the two issues, a distributed estimation structure with a moving activation policy (depicted in Fig. 7) can be developed and applied to the robotic UV curing process.

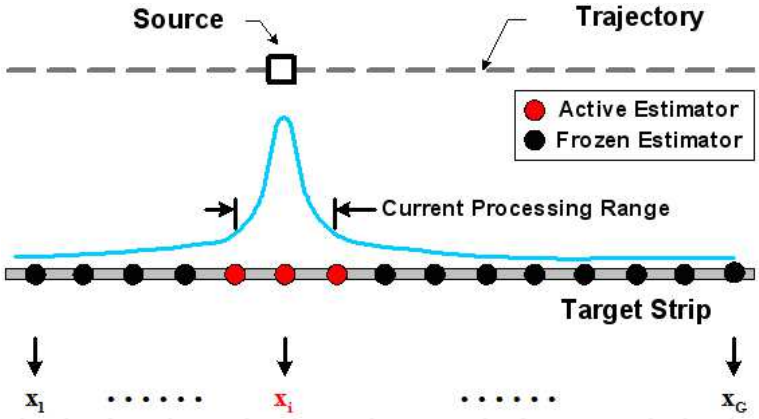

Fig. 7. The distributed estimation structure and the moving activation policy

In the distributed estimation structure shown in Fig. 7, the original process state vector x (describing the monomer concentration distribution along the whole target strip) is divided into a set of low-order subsystems which are denoted by $x_1,\cdots,x_i,\cdots,x_G$ (each of these subsystems only describes the local monomer concentration distribution around its own location), respectively. In these subsystems, only those that are located within the current processing range of the radiant source will be activated for the DEKF estimation, and the others are kept frozen at this time. As the radiant source moves through the target strip,

each subsystem will be activated sequentially to provide state and parameter estimation for the current processing range during the whole process. The distributed estimation structure described above can help reduce the computational cost thanks to the reduction of the dimension of the DEKF estimator. Meanwhile, since the moving activating policy ensures that the state/parameter estimation is only applied to the current processing range (subsystems within this range have better observabilty than other areas of the target strip), it can help compensate for the changing observability caused by the movement of the radiant source. The next subsection will give an example to demonstrate the DEKF estimation scheme developed for the robotic UV curing application.

3.3 Estimation results

In this subsection, simulation results are presented to illustrate the implementation of the DEKF estimation scheme to a 1D robotic UV curing example. In this example, the state to be estimated is the monomer concentration distribution (further normalized to the cure-conversion level) along the 1D target strip. Two unknown process parameters are considered here: UV absorption coefficient k and convective heat transfer coefficient h (the two parameters are estimated simultaneously). The assumed spatial distributions of the two parameters along the target strip are illustrated in Fig. 8.

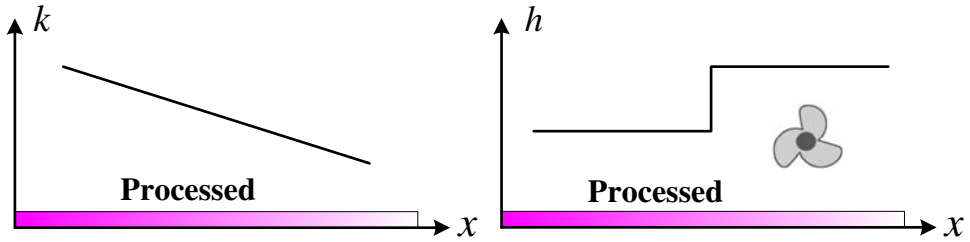

Fig. 8. Assumed distribution of the UV absorption coefficient and convective heat transfer coefficient along the 1D target strip

As shown in Fig. 8, the UV absorption coefficient is assumed to decrease in a linear manner from the left end to the right end of the target strip. For the convective heat transfer coefficient, a cooling fan is assumed to operate on the right-half part of the target strip, and a step function is used to describe the corresponding distribution of the convective heat transfer coefficient. Since this example is only used to demonstrate the estimation scheme (not the control strategy), the inputs of the system (motion and power of the radiant source) are kept constant during the whole process. Other process parameters used in this example are obtained from (Hong, 2004). The corresponding results are presented in Fig. 9 ~ Fig. 11. The solid ball shown in Fig. 9 ~ Fig. 11 denotes the UV radiant source which moves through the target strip (from left to right). The state estimation result is given in Fig. 9 in both the spatial (a) and temporal (b) domains. The shaded area in Fig. 9(a) represents the current processing (activating) window in which the corresponding local low-order estimators are activated for estimating the states and parameters. The time index t_L and t_R in Fig. 9(b) define the time when the estimation is activated and when it is frozen again for the selected position (x=0.9). t_M represents the time when the radiant source is exactly crossing the position (x=0.9). The spatial and temporal results in Fig. 9 show that the estimated state (cure-conversion level) has a good match to the actual state.

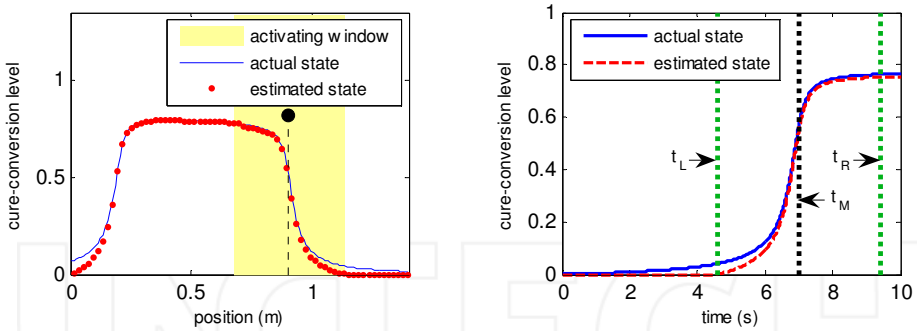

Fig. 9. (a) The distribution of the cure-conversion level along the target strip when the source is crossing the position (x=0.9m) (b) The time history of the cure-conversion level for the position (x=0.9m)

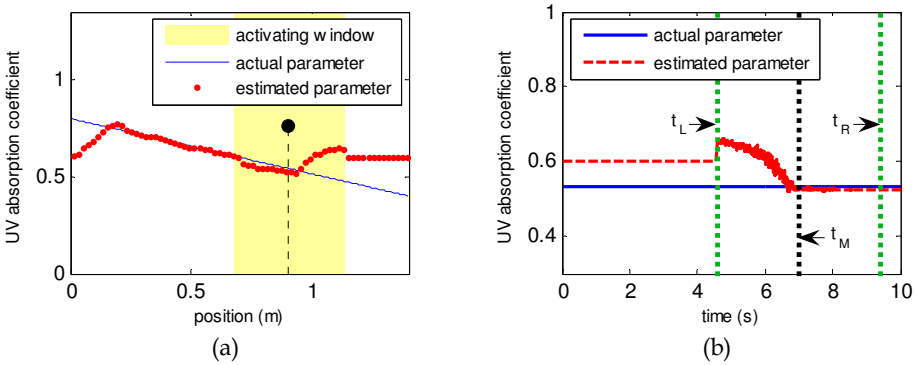

Fig. 10. (a) The distribution of the UV absorption coefficient along the target strip when the source is crossing the position (x=0.9m) (b) The time history of the UV absorption coefficient for the position (x=0.9m)

The estimation results for the UV absorption coefficient are given in Fig. 10. First, Fig. 10 (a) shows the spatial distributions of the estimated and actual UV absorption coefficient. It can be observed that the estimation performance for the cured area (on the left-hand side of the source) is better than that of the uncured areas (on the right-hand side of the source). This is because the estimation for the uncured areas hasn't been activated or it is currently being activated. Similar observations can be found in the temporal result depicted in Fig. 10 (b).

Fig. 11 presents the estimation results for the convective heat transfer coefficient. Again, for those areas in which the estimation has been activated, the estimated convective heat transfer coefficient matches the actual value well. On the other hand, for those areas covered by frozen estimators or the ones that are being activated, the estimation performance is not good at the beginning but is improved after the estimators have been completely activated.

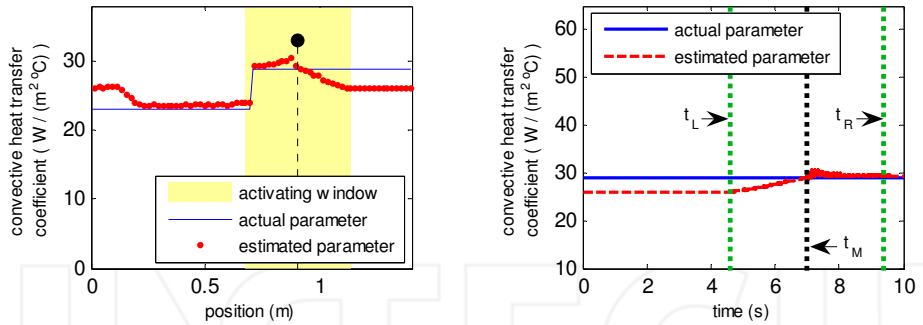

Fig. 11. (a) The distribution of the convective heat transfer coefficient along the target strip when the source is crossing the position (x=0.9m) (b) The time history of the convective heat transfer coefficient for the position (x=0.9m)

4. Process optimization and predictive control

To further improve quality and energy efficiency, optimization of multiple control inputs should be incorporated into the closed-loop control of the robotic UV curing process. This section presents two fundamental approaches to achieve the process optimization through either a rule-based control method or a model predictive control (MPC) strategy. A general discussion about the two approaches is given at first. Then the authors propose a framework for guiding the design of the predictive control strategy. Finally, a demonstrative example is provided to illustrate and compare the two process optimization approaches.

4.1 Off-line and online process optimization

The robotic UV curing process involoves two major control inputs: the power and motion of the radiant source. The control of a single manipulated variable (either the power or the motion) based on temperature feedback has been discussed in Secition 2. To achieve improved quality level and energy efficiency, the two control inputs should be manipulted in a coordinated and optimal manner. Two approaches are considered for achieving such process optimization: a rule-based control method (off-line optimization) and a model predictive control strategy. Both of the two approaches use essential process feedback provided by the state/parameter estimator.

4.1.1 Rule-based control

The rule-based control method is still a closed-loop control approach that uses some off-line process optimization results. The first step is to calculate the optimal trajectories of the two control inputs in an open-loop manner. For example, for curing a 1D target strip, the optimal trajectories of the two control inputs could be two constant values of the power and the speed (motion) which can minimize the pre-defined objective function (e.g. minimal curing level non-uniformity with minimal energy use). However, these off-line optimal control trajectories cannot be directly applied to the process due to the presence of disturbances during the actual process. Therefore, the next step is to close the loop by incorporating online process estimates and coordinating the control inputs based on some

designed rules. Although this method is not necessary optimal once the loop has been closed (the control inputs will be adjusted around the off-line optimal results), it can help achieve an acceptable compromise between process optimization and disturbance rejection.

4.1.2 Model predictive control

The other approach is to use model predictive control (MPC) to achieve online process optimization. Compared to the rule-based control method, the MPC approach calculates the optimal control inputs in a frequent manner by using online process estimates and a process model. The process model is used to predict future process states from the current state estimates. At each calculateion cycle, the MPC controller determines the control inputs in an optimal way that can minimize the deviation of future process states from the set-point and the corresponding control costs. This calcuation is repeated to generate new optimal control signals once the new state estiamtes are available, so the controller can detect the changes of the process (e.g. influence of disturbances) online and make necessary adjustment to compensate for these changes. The two process optimization approaches discussed above are illustrated in Fig. 12.

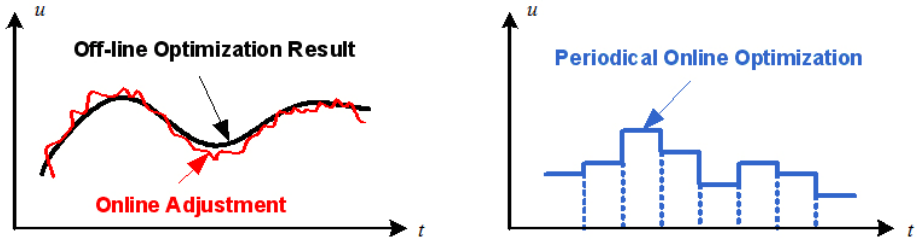

(a) (b)

Fig. 12. (a) The rule-based control method (b) The predictive control strategy

4.2 Predictive control strategy

This subsection presents a framework for developing the predictive control strategy for the robotic UV curing process. This framework outlines the fundamental procedures in the control design process, including model linearization and simplification, control problem formulation, solution, and implementation, etc. The basic structure of this framework is depicted in Fig. 13.

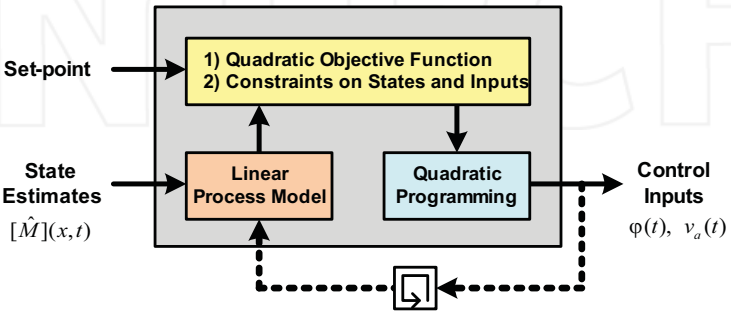

Fig. 13. The structure of the model predictive control framework for robotic UV curing

The steps involved in the predictive control strategy are described as follows:

1. Acquire new state estimates (monomer concentration) from the DEKF estimator discussed in Section 3.
2. Linearize the process model around the current state estimates and the previous control inputs.
3. Calculate future process states along the prediction horizon by using the linear model
4. Update the objective function and constraints on both states and inputs.
5. Solve the constrained optimization problem to find the optimal sequence of control inputs along the control horizon.
6. Apply the first part of the optimal sequence as the current control inputs to the process.

The above calculation will be repeated when the new state estimates are available. The detailed mathematical derivation and formulation of the predictive control strategy can be found in the authors' previous work in (Zeng & Ayalew, 2010-b).

4.3 A demonstrative example

This subsection provides a 1D curing example to demonstrate the rule-based control method and the predictive control strategy as used for process optimization. Two simulation scenarios (named as S1 and S2) are given in this example, regarding different disturbances in the UV absorption coefficient distribution along the target strip. For the first scenario (S1), the UV absorption coefficient has the same distribution as what is shown in Fig. 8. For the second scenario (S2), the distribution of the UV absorption coefficient is described by a step function. The simulation results for S1 are presented in Fig. 14 and Fig. 15.

As shown in Fig. 14, both the rule-based and predictive control methods successfully maintain the uniformity of the cure-conversion level along the target strip, although the UV absorption coefficient has a descending distribution. The open-loop method fails to maintain the uniformity due to the lack of essential process feedback. Fig. 15 gives the time history of the two major control inputs: power and motion. It can be observed that for both the rule-based and predictive control methods, the power of the radiant source is increased while the speed of the source is reduced during the process. This explains why the two closed-loop methods can compensate for the disturbance in the UV absorption coefficient.

The simulation results for S2 are presented in Fig. 16 and Fig. 17.

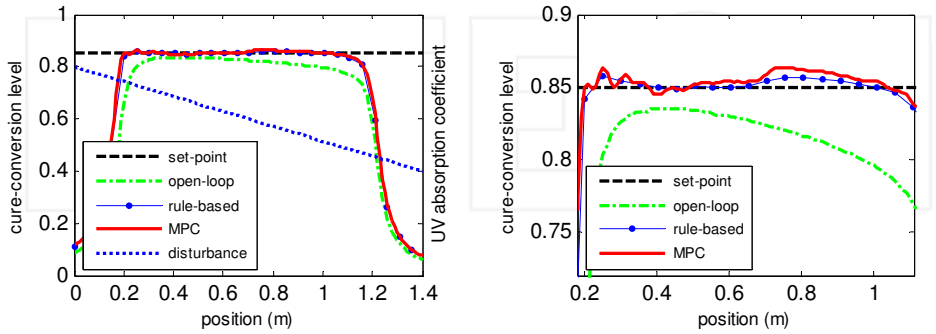

Fig. 14. The distribution of the cure-conversion level along the target strip (S1): (a) Full-range view (b) Zoomed view around the set-point

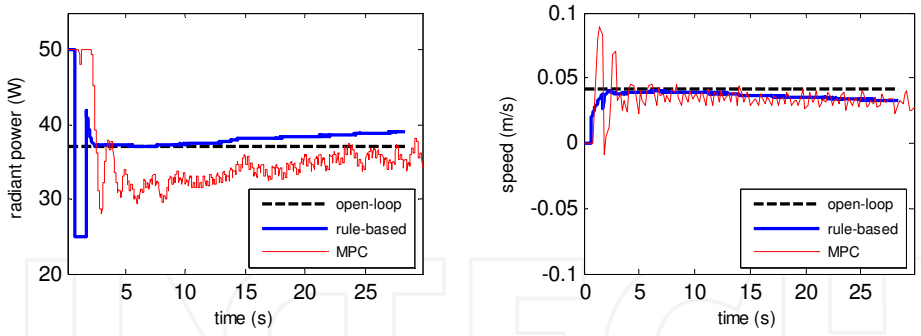

(a) (b)

Fig. 15. The time history of the control inputs (S1): (a) radiant power (b) speed

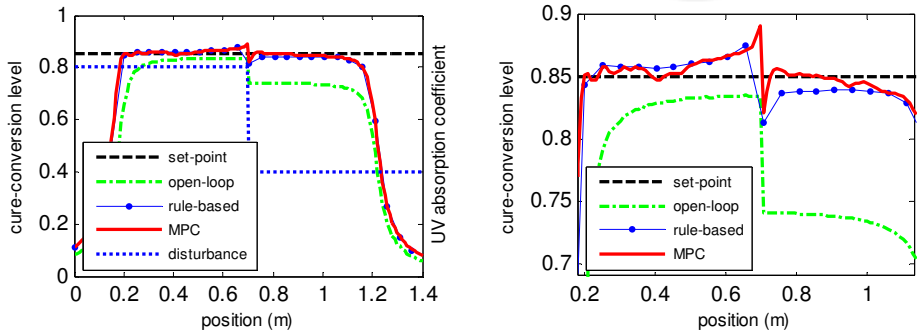

(a) (b)

Fig. 16. The distribution of the cure-conversion level along the target strip (S2): (a) Full-range view (b) Zoomed view around the set-point

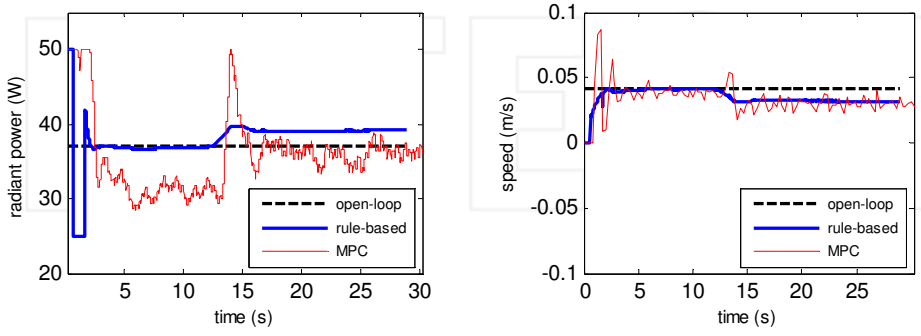

(a) (b)

Fig. 17. The time history of the control inputs (S2): (a) radiant power (b) speed

In this scenario, a step change is introduced to the distribution of the UV absorption coefficient along the target strip (as shown in Fig. 16). Similarly, the rule-based and the predictive control methods successfully compensate for this step change and give acceptable process uniformity, compared to the uneven curing in the open-loop method. The time history of the control inputs given in Fig. 17 shows that the power and the speed of the radiant source are also manipulated in a step manner during the process (for both the rule-based and the predictive control methods). It can be observed that the predictive control method increases the radiant power more drastically than the rule-based method does when the radiant source crosses the step point. This is because the predictive control strategy can detect the step change in advance and make corresponding adjustment in time. Another observation is that the predictive strategy uses lower radiant power than the rule-based method at most time of the curing process. This explains the major difference between the two process optimization approaches. Since the predictive control strategy performs the optimization online, it can give better energy efficiency (minimize power level) than the rule-based method which only uses off-line optimization results to determine nominal values of the control inputs.

5. A prototype robotic UV curing system

A prototype robotic UV curing system has been developed to implement the closed-loop control methods in experiment and investigate their potential applications in automotive manufacturing plants. The hardware structure of the prototype robotic UV curing system is illustrated in Fig. 18.

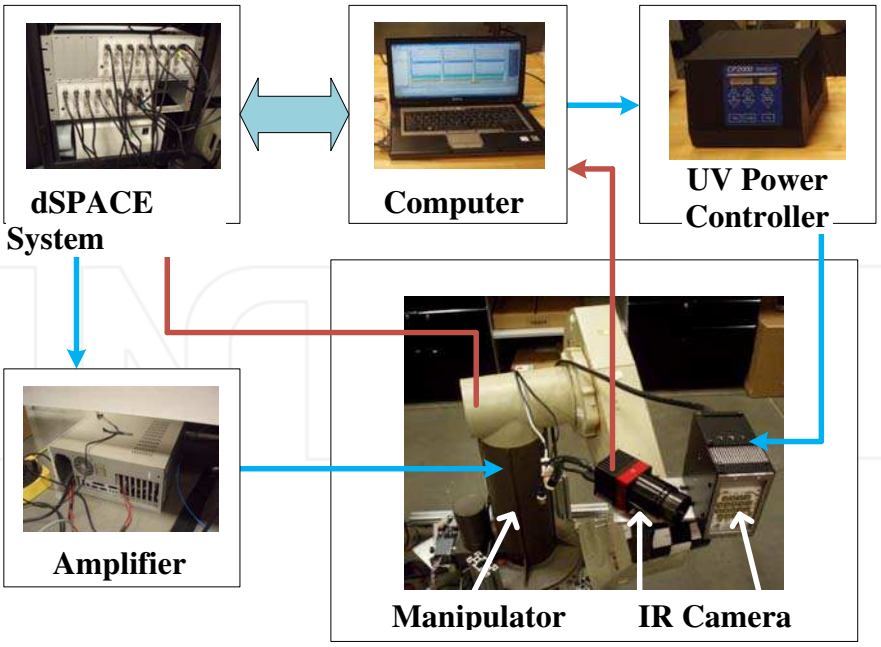

Fig. 18. The hardware structure of the prototype robotic UV curing system

As shown in Fig. 18, the prototype system is composed of four basic parts: a robotic manipulator, a UV LED panel with power controller, a thermal vision system, and a dSPACE rapid control prototyping system. A six degree-of-freedom (DOF) PUMA560 manipulator is used here to carry the UV LED panel and the IR camera. This manipulator is driven by six new pulse-width modulation (PWM) amplifiers. The UV LED panel includes 42 cells which can send out UV radiation with a wavelength concentrated around 365 nm. The UV LED is connected with its own power controller (named CF2000). This controller can be treated as an instrument terminal of a personal computer (PC) through a USB interface. The IR camera used in the prototype system has a 640×320 pixel array and can measure the temperature from 20 to 150 °C. The IR camera is connected with the computer through a USB interface and it can send out digital thermal image data at a frame rate of 30Hz. The dSPACE system includes an embedded processor and necessary A/D and D/A converters. The dSPACE system is used to achieve rapid control prototyping by converting MATLAB/Simulink control models into real-time codes that can be implemented in hardware to control the whole system.
Fig. 19 shows two test configurations with the prototype robotic UV curing system.

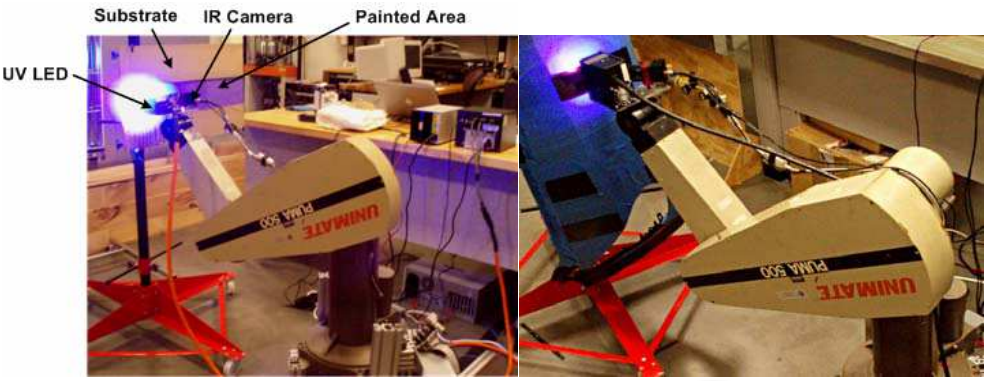

(a) (b)

Fig. 19. Test configurations with the prototype robotic UV curing system: (a) 2D plane-type target (b) Actual automotive body part (a front fender)

At first, the prototype system is used to cure a 2D plane-type target (with thin-film clearcoat) for validating the temperature feedback control strategy discussed in Section 2. It can also be used to cure some real automotive body parts, such as a front fender, as shown in Fig. 19(b). In this case, the trajectory of the robot is typically designed offline to make the UV LED panel have different distances matched to the profile of the fender as it moves through different locations. With the closed-loop structure, the controller can determine how long the UV LED panel should stay at each patch of the fender based on the temperature level of that patch as measured by the IR camera.

6. Summary and future directions

This chapter presented a framework for advanced robotic radiative process control in automotive coating, drying and curing applications. This framework provides potential solutions to the closed-loop control problems, particularly to those involved in the robotic UV curing processes. These solutions include, 1) online process monitoring through IR camera(s) and direct temperature feedback control, 2) online process state/parameter estimation by using temperature measurements and the dual extended Kalman filtering, and 3) process optimization through rule-based and predictive control methods. Simulation studies have been conducted to demonstrate the major approaches discussed in this chapter. The results show that the proposed framework (control, estimation, and optimization) provides improved process quality and energy efficiency by adaptively compensating for disturbances and optimally coordinating multiple control inputs (power and motion). A prototype system has also been established for further investigations and implementations on robotic UV curing for automotive applications.

Future research work will include implementing the state/parameter estimation schemes and the predictive control strategy in hardware, conducting investigations on advanced UV radiant sources for more control options, and pursuing the cooperation with manufacturers for further on-site tests and applications.

7. References

Ashdown, I. (1994). *Radiosity: A Programmer's Perspective*, John Wiley and Sons, New York, NY.

Fey, T. and Muhle, J. (2003). UV-dualcure systems for automotive applications. RadTech, 2003, Berlin, Germany.

Goodner, M.D. and Bowman, C.N. (2002). Development of a comprehensive free radical photopolymerization model incorporating heat and mass transfer effects in thick films. *Chemical Engineering Science*, Vol. 57, No. 5, pp. 887-900.

Hagood, D., Kelly, M. (2008). Extolling the advantages of UV-Curing processes. *Metal Finishing*, Vol. 106, No. 4, pp. 71-74.

Hardt, D.E. (1993). Modeling and control of manufacturing processes: Getting more involved. *Transactions of the ASME. Journal of Dynamic Systems, Measurement and Control*, Vol. 115, No. 2B, pp. 291-300.

Haykin, S.S. (2001). *Kalman filtering and neural networks*, John Wiley and Sons, New York, NY.

Hong, W., Lee, Y.T., and Gong, H. (2004). Thermal analysis of layer formation in a stepless rapid prototyping process. *Applied Thermal Engineering*, Vol. 24, No. 2-3, pp. 255-268.

Huissoon, J.P., Strauss, D.L., Rempel, J.N., Bedi, S., and Kerr, H.W. (1994). Multi-variable control of robotic gas metal arc welding. *Journal of Materials Processing Technology*, Vol. 43, No. 1, pp. 1-12.

Jones, P.D.A., Duncan, S.R., Rayment, T., and Grant, P.S. (2003). Control of temperature profile for a spray deposition process. *IEEE Transactions on Control Systems Technology*, Vol. 11, No. 5, pp. 656-667.

Kalman, R.E. (1960). A new approach to linear filtering and prediction problems. *Transactions of the ASME–Journal of Basic Engineering*, Series D, Vol. 82, pp. 35–45.

Mills, P. (2001). Team UV: Leading edge technology for the automotive industry. RadTech, 2001, Basel, Switzerland.

Mills, P. (2005). Robotic UV curing for automotive exterior applications: A cost-effective and technically viable alternative for UV curing. North American Automotive UV Consortium Report, Stongsville, OH.

Modest, M.F. (1993). *Radiative Heat Transfer*, McGraw Hill, New York, NY.

Moore, K.L., Naidu, D.S., Yender, R., and Tyler, J. (1997). Gas metal arc welding control: Part I : Modeling and analysis. *Nonlinear Analysis, Theory, Methods and Applications*, Vol. 30, No. 5, pp. 3101-3111.

Omar, M. A., Viti, V., Saito, K., and Liu, J. (2006). Self-adjusting robotic painting system. *Industrial Robot: An International Journal*, Vol. 33, No. 1, pp. 50-55.

Prendi, L. and Tam, Edwin K.L. (2008). Life cycle inventory of the automotive paint process. *Journal of Coatings Technology*.

Seelinger, M.J., Robinson, M., Dieck, Z., and Skaar, S.B. (1997). A vision-guided, semi-autonomous system applied to a robotic coating application. in *Proceedings of the SPIE - The International Society for Optical Engineering*, Vol. 3209, pp. 133-144.

Siewert, U. (2008). Solutions for energy and environmental issues in automobile manufacturing, in *Durr Investor's Day*, 2008, Darmstadt, Germany.

Starzmann, O. (2001). UV-light curing in the automotiveindustry. RadTech, 2001, Basel, Switzerland.

Raith, T., Bischof, M., Deger, M., Gemmler, E. (2001). 3-D UV technology for OEM coatings. RadTech, 2001, Basel, Switzerland.

U.S. Department of Energy, Office of Industrial Technologies, Energy Efficiency and Renewable Energy (2003). Progressive powder coating: New infrared curing oven at metal finishing plant increases production by 50% (BestPractices Case Study).

U.S. Department of Energy, Office of Industrial Technologies, Energy Efficiency and Renewable Energy (1999). UV-Curable coatings for aluminum can production (Chemicals Project Fact Sheet).

Vogt, M. (2007). Infrared drying lowers energy costs and drying times. *Plastics, Additives and Compounding*, Vol. 9, No. 5, pp. 58-61.

Wan, E.A. and Nelson, A.T. (1997). Neural dual extended Kalman filtering: applications in speech enhancement and monaural blind signal separation. Neural Networks for Signal Processing VII., in *Proceedings of the 1997 IEEE Signal Processing Society Workshop*, pp. 466-475.

Zeng, F., Ayalew, B., and Omar, M. A. (2009). Robotic automotive paint curing using thermal signature feedback. *Industrial Robot: An International Journal*, Vol. 36, No. 4, pp. 389-395.

Zeng, F. and Ayalew, B. (2010-a). Estimation and coordinated control for distributed-parameter processes with a moving radiant actuator. *Journal of Process Control*, Vol. 20, No. 6, pp. 743-753.

Zeng, F. and Ayalew, B. (2010-b). Model predictive control of a distributed parameter process employing a moving radiant actuator. ASME Dynamic Systems and Control Conference, Cambridge, MA, USA, September 13-15, 2010 (accepted).

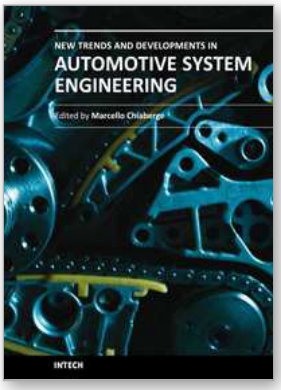

New Trends and Developments in Automotive System Engineering

Edited by Prof. Marcello Chiaberge

ISBN 978-953-307-517-4
Hard cover, 664 pages
Publisher InTech
Published online 08, January, 2011
Published in print edition January, 2011

In the last few years the automobile design process is required to become more responsible and responsibly related to environmental needs. Basing the automotive design not only on the appearance, the visual appearance of the vehicle needs to be thought together and deeply integrated with the â€œpowerâ€ developed by the engine. The purpose of this book is to try to present the new technologies development scenario, and not to give any indication about the direction that should be given to the research in this complex and multi-disciplinary challenging field.

How to reference

In order to correctly reference this scholarly work, feel free to copy and paste the following:

Fan Zeng and Beshah Ayalew (2011). Advanced Robotic Radiative Process Control for Automotive Coatings, New Trends and Developments in Automotive System Engineering, Prof. Marcello Chiaberge (Ed.), ISBN: 978-953-307-517-4, InTech, Available from: http://www.intechopen.com/books/new-trends-and-developments-in-automotive-system-engineering/advanced-robotic-radiative-process-control-for-automotive-coatings

INTECH
open science | open minds

InTech Europe
University Campus STeP Ri
Slavka Krautzeka 83/A
51000 Rijeka, Croatia
Phone: +385 (51) 770 447
Fax: +385 (51) 686 166
www.intechopen.com

InTech China
Unit 405, Office Block, Hotel Equatorial Shanghai
No.65, Yan An Road (West), Shanghai, 200040, China
中国上海市延安西路65号上海国际贵都大饭店办公楼405单元
Phone: +86-21-62489820
Fax: +86-21-62489821